

Short Range Correlations and Spectral Functions in Asymmetric Nuclear Matter

P. Konrad, H. Lenske, U. Mosel

Institut für Theoretische Physik, Universität Gießen
Heinrich-Buff-Ring 16, D-35392 Gießen, Germany

October 25, 2019

Abstract

Dynamical correlations in asymmetric infinite nuclear matter are investigated in a transport theoretical approach. Self-energies due to short range correlations and their influence on the nucleon spectral functions are described in an approach accounting for a realistic treatment of mean-field dynamics and a self-consistently derived quasi-particle interaction. Landau-Migdal theory is used to derive the short range interaction from a phenomenological Skyrme energy density functional. The spectral functions in asymmetric nuclear matter are found to follow in their gross features closely the patterns observed previously in symmetric nuclear matter. An interesting sensitivity of dynamical self-energies and spectral functions on the momentum structure of the underlying interactions is found.

1 Introduction

Correlations beyond those described by the static mean-field are of genuine interest for the understanding of the dynamics in a nuclear many-body system. Although experience seems to confirm the prevalence of mean-field dynamics and the directly related quasi-particle picture a closer inspection reveals that nucleons in matter obey more involved rules. For symmetric nuclear matter this has been discussed extensively in the literature, e.g. in a recent review [1], and also was considered in our previous work [2, 3, 4]. However investigations for asymmetric nuclear matter are rare. Some of the few cases are [5] and [6]. In symmetric matter and stable finite nuclei one finds typically a suppression of the quasi-particle strength by about 10%. Pure

mean-field dynamics predicts that in nuclear matter the spin- and momentum states are uniformly occupied inside the Fermi-sphere up to the sharp surface at the Fermi-momentum k_F . Hence, the momentum distribution $n_q(k)$ for protons and neutrons ($q=p,n$), respectively, up to a normalization constant is described appropriately by a step function, $n_q(k) \sim \theta(k_F^q - k)$ where $k_F^p = k_F^n$ for symmetric nuclear matter. As a matter of fact, in a more realistic description, going beyond the mean-field, this pattern changes. The nucleons cease to be in sharp energy-momentum states but acquire spectral functions of a finite width, thus resolving the strict on-shell relation between energy and momentum. Hence, the mean-field configurations only exist with a finite life time, determined by the strength of the coupling to $2h - 1p$ and $1p - 2h$ states, respectively. Correspondingly, in finite nuclei one observes a reduction of single particle spectroscopic factors when going away from the Fermi level. More dramatic effects are found in exotic nuclei. Leaving the valley of stability, the experiments [7, 8] and theory [9, 10] agree in observing strongly suppressed single particle probabilities already close to the Fermi level of neutron-rich nuclei.

Despite the fact that strongly asymmetric exotic nuclei are of central interest for modern nuclear structure physics, the contributions of short range correlations to asymmetric nuclear matter and finite nuclei is still a rarely touched problem in nuclear physics. Short range correlations play an important role for the understanding of nuclear matter as for example seen in the observed high energy tails of nuclear momentum distributions and form factors. Also, short range correlations play a decisive role in understanding the structure of finite nuclei, particle production in heavy ion collisions and astrophysical objects like supernovae. Since supernovae are highly asymmetric in isospin we need a more detailed knowledge of correlations in asymmetric matter beyond ordinary mean-field interactions.

Here, our main goal is to explore the interplay of mean-field dynamics and correlations in asymmetric nuclear matter. It is worthwhile to recall that in asymmetric matter isovector interactions are giving rise to strongly asymmetric Fermi energies for proton and neutrons. Hence, as an immediate consequence the available density of states of excited states changes, becoming increasingly different for proton and neutron configurations, respectively, with changing proton-to-neutron ratio. This a new aspect, clearly not accessible in the conventional approaches concentrating on symmetric nuclear matter.

From our previous work we know that the spectral functions in symmetric nuclear matter are determined by interactions of extremely short range which are very well approximated by point couplings, reproducing almost perfectly results from rather involved many-body calculations, e.g. in [11], both for

cold [2, 3] and hot [4] symmetric matter at all densities. It is therefore tempting to extend the same transport theoretical approach to asymmetric nuclear matter.

Long-range mean-field effects are included by a Skyrme energy functional by which we account for the above mentioned change in the Fermi-energies of protons and neutrons, respectively. The basic transport theoretical relations are summarized in section 2 and are extended to the general case of asymmetric nuclear matter. We also discuss the influence of charge asymmetry on the mean-field, affecting both the effective mass and the effective binding potentials in asymmetric matter. Landau-Migdal theory is used to estimate the matrix elements for the ppp^{-1} , nnn^{-1} , pnn^{-1} and npp^{-1} collisions by which the dissipation of spectral single particle strength is determined. Results of transport calculations for the spectral functions, self-energies and momentum distributions of protons and neutrons in asymmetric nuclear matter at various degrees of neutron excess are presented in section 3. Finally we will close in section 4 with a summary and an outlook.

2 Spectral Functions in Asymmetric Nuclear Matter

The underlying model for our calculations was presented in [2, 3] and used for calculations in cold ($T = 0$) symmetric nuclear matter at saturation point density ρ_0 and for finite temperature and high densities in [4]. At this point we restrict ourselves to a short summary of the formalism with a few changes in respect to asymmetric nuclear matter. For a more detailed calculation see [2, 3, 4].

The two-particle-one-hole (2p1h) and one-particle-two-hole (1p2h) polarization self-energies $\Sigma^>$ and $\Sigma^<$ for nucleons in nuclear matter are given by [12]:

$$\begin{aligned} \Sigma_q^{\gtrless} = & g \sum_{q'} \int \frac{d^3 k_2 d\omega_2}{(2\pi)^4} \frac{d^3 k_3 d\omega_3}{(2\pi)^4} \frac{d^3 k_4 d\omega_4}{(2\pi)^4} (2\pi)^4 \delta^4(k + k_2 - k_3 - k_4) \overline{|M_{qq'}|^2} \\ & \times g_{q'}^{\lessgtr}(\omega_2, k_2) g_q^{\gtrless}(\omega_3, k_3) g_{q'}^{\gtrless}(\omega_4, k_4) \end{aligned} \quad (1)$$

where $g = 2$ is the spin degeneracy. Compared to symmetric nuclear matter neutrons and protons occupy different Fermi spheres, which leads to different self-energies. In the asymmetric case one has to account for collisions with particles of the same kind (pp and nn) and for collisions with particles of different kind (pn and np). This explains the summation over the isospin q' in equation (1).

The one particle correlation function g_q^{\gtrless} in equation (1) can be expressed in terms of spectral functions

$$\begin{aligned} g_q^<(\omega, k) &= ia_q(\omega, k)\theta(\omega_q - \omega), \\ g_q^>(\omega, k) &= -ia_q(\omega, k)(1 - \theta(\omega_q - \omega)), \end{aligned} \quad (2)$$

where ω_q is the Fermi energy of the nucleons and $\theta(\omega_q - \omega)$ the step function to account the Fermi distribution in case of cold nuclear matter. The nonrelativistic spectral function for nucleons is found explicitly as,

$$a_q(\omega, k) = \frac{\Gamma_q(\omega, k)}{(\omega - \frac{k^2}{2m_q} - \Sigma_q^{mf} - \text{Re}\Sigma_q^{ret}(\omega, k))^2 + \frac{1}{4}\Gamma_q^2(\omega, k)}, \quad (3)$$

where $\text{Re}\Sigma_q^{ret}(\omega, k)$ is the real part of the retarded self-energy, which can be calculated dispersively:

$$\text{Re}\Sigma_q^{ret}(\omega, k) = P \int \frac{d\omega'}{2\pi} \frac{\Gamma_q(\omega', k)}{\omega' - \omega} \quad (4)$$

The width $\Gamma_q(\omega, k)$ is given by the imaginary part of the retarded self-energy,

$$\Gamma_q(\omega, k) = 2\text{Im}\Sigma_q^{ret} = i(\Sigma_q^>(\omega, k) - \Sigma_q^<(\omega, k)). \quad (5)$$

We introduce the asymmetry coefficient

$$\xi = \frac{\rho_p}{\rho_n + \rho_p} \quad (6)$$

which indicates the fraction of protons at a given total nucleon density $\rho = \rho_n + \rho_p$, where ρ also is the iso-scalar nucleon density. To see the influence of asymmetry we split the mean-field in proton and neutron contributions:

$$\Sigma_p^{mf} = \Sigma_{pp}^{mf} + \Sigma_{pn}^{mf} = \rho\xi u_{pp} + \rho(1 - \xi)u_{pn} \quad (7)$$

$$\Sigma_n^{mf} = \Sigma_{nn}^{mf} + \Sigma_{np}^{mf} = \rho(1 - \xi)u_{nn} + \rho\xi u_{np}. \quad (8)$$

Σ_{pp}^{mf} and Σ_{np}^{mf} are generated by the proton background, which vanishes for pure neutron matter. Σ_{nn}^{mf} and Σ_{pn}^{mf} are generated by the neutron background. On the right hand side u_{pp} and u_{pn} are effective interactions averaged over the proton Fermi sphere for u_{pp} and the neutron Fermi sphere for u_{pn} in phase space. The same for u_{np} and u_{nn} .

One can easily see in equation (8) that there is no difference for neutrons and protons in case of symmetric nuclear matter ($\xi = 0.5$) and one has not

to distinguish between protons and neutrons. Going over to the asymmetric case the mean-field contributions split up, now protons and neutrons are distinguishable by their different dynamical laws. Absorbing the momentum dependent part of the mean-field up to second order in k into the kinetic energy term

$$\hbar^2 \frac{k^2}{2m} + \Sigma_q^{mf}(k, \rho) \cong \hbar^2 \frac{k^2}{2m_q^*} + U_q^{eff}(\rho) \quad (9)$$

leads to an effective mass m_q^* and an momentum-independent effective potential U_q^{eff} . Starting with symmetric matter, where the effective masses and effective potentials are the same, for p and n , respectively, the masses and potentials for nucleons of different isospin start to split up for asymmetric matter. As seen in equation (3) the mean-field contribution plays an important role for the spectral function's pole structure. Hence, we expect a separation of the proton and neutron quasiparticle peaks.

We account for mean-field effects in our model by means of a Skyrme energy density functional with parameters taken from the recent set of ref. [16]. By executing the variation with respect to the kinetic energy density τ_q and the nucleon density ρ_q , where $q = n, p$ one obtains for the effective mass and for the effective potential:

$$\frac{m_q}{m_q^*} = 1 + \frac{2m_q}{\hbar^2} \left(\frac{1}{8} [t_1(2+x_1) + t_2(2+x_2)] \rho \right. \quad (10)$$

$$\left. + \frac{1}{8} [t_2(2x_2+1) - t_1(2x_1+1)] \rho_q \right)$$

$$U_q^{eff} = \frac{1}{4} t_0 [2(2+x_0)\rho - 2(2x_0+1)\rho_q]$$

$$\frac{1}{24} t_3 \rho^\sigma [2(2+x_3)\rho - 2(2x_3+1)\rho_q]$$

$$\frac{1}{24} \sigma t_3 \rho^{\sigma-1} [(2+x_3)\rho^2 - (2x_3+1)(\rho_p^2 + \rho_n^2)]$$

$$\frac{1}{8} [t_1(2+x_1) + t_2(2+x_2)] \tau$$

$$\frac{1}{8} [t_2(2x_2+1) - t_1(2x_1+1)] \tau_q \quad (11)$$

where ρ is the total and τ total kinetic density. The Skyrme parameters x_0 , x_1 , x_2 , x_3 , t_0 , t_1 , t_2 , t_3 and σ are given in table 1.

In the numerical calculations we use an iterative approach. Starting with an initial choice for the widths, i.e the imaginary part of the self-energy, we calculate the spectral functions, which then serve as input for re-calculating

t_0 ($MeV \cdot fm^3$)	-2490.23
t_1 ($MeV \cdot fm^5$)	489.53
t_2 ($MeV \cdot fm^5$)	-566.58
t_3 ($MeV \cdot fm^{3+3\sigma}$)	13803.0
x_0	1.1318
x_1	-0.8426
x_2	-1.0
x_3	-1.9219
σ	-1/6
W_0 ($MeV \cdot fm^5$)	131.0

Table 1: The parameters of the Skyrme SLy230a [16] interaction. The spin-orbit parameter W_0 is included for completeness only.

the self-energies. These results are used as input for the next step of an iterative calculation, thus improving the results. The calculation is stopped, when the spectral functions are converged to a given accuracy. In the language of Feynman diagrams this approach corresponds to the summation of the sunset diagram to all orders [3].

2.1 The Short Range Interaction

The former investigations were restricted to symmetric nuclear matter at saturation density. That highly symmetric situation simplifies the calculations because protons and neutrons are indistinguishable. Irrespective of the charge state, spectral functions and other observables can be related to a universal Fermi level, common to protons and neutrons. As pointed out before, in asymmetric matter the isovector mean-field changes the situation completely by introducing a relative shift of the proton and neutron Fermi surfaces, in addition to the changes from the differences in particle number. Also, by following the shift of the equilibrium density with increasing asymmetry, here we have to have information on the value of $|\overline{M}_{qq'}|^2$ at changing total number densities. However, from our former work we expect that only the short range parts of the full in-medium NN interaction will be relevant.

An appropriate approach to investigate this aspect and, as an important side aspect, to test the consistency with the mean-field part of the model calculations we use Landau-Migdal theory [13]. Given an energy density functional $\mathcal{E}(\rho)$ Landau-Migdal theory provides a way to calculate the corresponding residual 2-quasiparticle interaction by second variation of $\mathcal{E}(\rho)$ with respect to the various spin and isospin densities [13, 14].

For a Skyrme energy density functional the resulting parameters $f_0(\rho)$, $f'_0(\rho)$, $g_0(\rho)$ and $g'_0(\rho)$, characterizing the interaction strength and density dependence in the spin-isospin $S = 0, T = 0$, $S = 0, T = 1$, $S = 1, T = 0$, $S = 1, T = 1$ s-wave ph interaction channels, are in fact derivable in closed form, e.g. [14]. According to the structure of the Skyrme energy density functional the Landau-Migdal parameters are constrained to monopole and dipole components.

However, these Skyrme values include short and long range interactions. The origin and nature of the various pieces cannot be identified directly. Here we are interested mainly in the short range parts. A simple but meaningful way to extract the short range parts is to identify the long range components with pion exchange. Consequently, we define the short range part of the interaction by subtracting from the interaction derived from the Skyrme energy density functional the (central part of) the pion exchange NN interaction. Hence, we use the central interaction obtained from pion exchange and include anti-symmetrization explicitly by means of the spin and isospin exchange operators $P_{\sigma,\tau}$, respectively, thus leading to

$$V_\pi(\vec{k}_1, \vec{k}_2) = -f_\pi^2 D_\pi(\vec{k}_1, \vec{k}_2) \vec{\sigma}_1 \cdot \vec{\sigma}_2 \vec{\tau}_1 \cdot \vec{\tau}_2 (1 - P_\sigma P_\tau) \quad , \quad (12)$$

which evidently can be arranged into

$$V_\pi(\vec{k}_1, \vec{k}_2) = \sum_{S,T=0,1} V_{ST}^{(\pi)}(\vec{k}_1, \vec{k}_2) (\vec{\sigma}_1 \cdot \vec{\sigma}_2)^S (\vec{\tau}_1 \cdot \vec{\tau}_2)^T \quad (13)$$

Above, the momentum space pion propagator is denoted by

$$D_\pi(\vec{k}_1, \vec{k}_2) = \frac{1}{(p^2 + m^2)} F(p^2) \quad (14)$$

including a monopole form factor with a cutoff $\Lambda = 800 \text{ MeV}/c$. The 3-momentum transfer is in the t-channel $\vec{p} = \vec{k}_2 - \vec{k}_1$ while in the u-channel we have $\vec{p} = \vec{Q} = \vec{k}_2 + \vec{k}_1$. Numerically, we use $f_\pi \simeq 0.075$ which is the standard value for the pseudo-vector πNN coupling constant.

Hence, we cast the energy density functional into the form

$$E(\rho) = E_s(\rho) + E_\pi(\rho) \quad (15)$$

where $E_s \equiv E - E_\pi$ is the short-range contribution. The long range pionic part E_π is given by a sum over the various spin and isospin transfer contributions as defined in eq.13. Formally E_π can be written as a sum over all spin-isospin channels

$$E_\pi(\rho) = \frac{1}{2} \sum_{q,q'=p,n} \sum_{S,T=0,1} \int \frac{d^3 k_1}{(2\pi)^3} \int \frac{d^3 k_2}{(2\pi)^3} \Theta(k_F(q) - k_1) \Theta(k_F(q') - k_2) \times V_{ST}^{(\pi)}(\vec{k}_1, \vec{k}_2) \langle (\vec{\sigma}_1 \cdot \vec{\sigma}_2)^S (\vec{\tau}_1 \cdot \vec{\tau}_2)^T \rangle \quad (16)$$

although in spin-saturated nuclear matter only the $S = 0$ are non-vanishing. In symmetric nuclear also the $T = 1$ components will not contribute. The brackets indicate traces over spin and expectation values on isospin and the step functions constrain the momentum integrals to the proton and neutron Fermi-spheres with Fermi-momenta $k_F(q)$, $q = p, n$, respectively.

Performing the variation with respect to the various spin and isospin densities we find in symmetric nuclear matter the set of Landau-Migdal parameters which in standard notation are

$$f_0^{(\pi)}(\rho) = -4\pi \frac{9}{4} N_0(k_F) \frac{f_\pi^2}{2k_F^2} Q_0(1 + \frac{m_\pi^2}{2k_F^2}) + f^{(r)}(k_F) \quad (17)$$

$$f_0'^{(\pi)}(\rho) = +4\pi \frac{3}{4} N_0(2k_F) \frac{f_\pi^2}{2k_F^2} Q_0(1 + \frac{m_\pi^2}{k_F^2}) \quad (18)$$

$$g_0^{(\pi)}(\rho) = +4\pi \frac{3}{4} N_0(k_F) \frac{f_\pi^2}{2k_F^2} Q_0(1 + \frac{m_\pi^2}{2k_F^2}) \quad (19)$$

$$g_0'^{(\pi)}(\rho) = 4\pi N_0(k_F) f_\pi^2 \left(\frac{1}{m_\pi^2} - \frac{1}{8k_F^2} Q_0(1 + \frac{m_\pi^2}{2k_F^2}) \right) \quad (20)$$

where $Q_0(z) = \frac{1}{2} \ln(\frac{1+z}{1-z})$ is the Legendre polynominal of second kind for $l = 0$. A more detailed calculation is found in the appendix. In the $S = 0, T = 0$ interaction channel an additional rearrangement term appears

$$f^{(r)}(k_F) = N_0(k_F) V_0^{(\pi)}(0, 0) h(k_F/m_\pi) \quad (21)$$

where $V_0^{(\pi)}(q, k)$ is the monopole component of the $S = 0, T = 0$ ph-u-channel pion exchange interaction and

$$h(z) = \frac{(1 + 2 z^2) \ln(1 + 4 z^2) - 4 z^2}{8z^4} \quad . \quad (22)$$

The Landau-Migdal parameters are pure numbers obtained by normalizing the interactions to the level density at the Fermi surface. We use $N_0(k_F) = 2k_F M^*/(\pi\hbar)^2$, leading to $1/N_0 = 154 \text{ MeV fm}^3$ at the saturation point with $k_F = 1.33 \text{ fm}^{-1}$.

The short range components are defined by subtracting the pion contributions, e.g. in the $(S = 0, T = 0)$ interaction channel:

$$f_0^{(s)}(\rho) = f_0(\rho) - f_0^{(\pi)}(\rho) \quad (23)$$

and $f_0'^{(s)}$, $g_0^{(s)}$ and $g_0'^{(s)}$ are defined accordingly. The $\ell = 0$ monopole Landau-Migdal Parameters for the full Lyon-4 interaction and the short range parameters after subtraction of the pion parts are displayed in Fig.2. While the

pion contributions are small in the $(S = 0, T = 1)$ and the $(S = 1, T = 0)$ channels, the $(S = 0, T = 0)$ and $(S = 1, T = 1)$ gain additional strength, being attractive in the first and repulsive in the second case.

The short range components are obtained by subtraction of the pion part from the full Landau-Migdal parameters, e.g. in the $S = 0, T = 0$ channel: $f_0^s(\rho) = f_0(\rho) - f_0^\pi(\rho)$ and correspondingly for the other channels. The matrix element relevant for our calculations is defined from the pp , nn , np and pn spin-scalar and spin-vector amplitudes, respectively,

$$f_{q'q}(\rho) = f_0(\rho) + (-)^{q'-q} f_0'(\rho); \quad (24)$$

$$g_{q'q}(\rho) = g_0(\rho) + (-)^{q'-q} g_0'(\rho) \quad (25)$$

by averaging over the spin degree of freedom. For the isospin projection quantum numbers we use $q = \pm \frac{1}{2}$ for neutrons and protons. Because of isospin symmetry we have $f_{pp} = f_{nn}$ and $f_{pn} = f_{np}$, respectively. Hence, we define

$$\overline{M}_{q'q}(\rho) = \frac{1}{4} (f_{q'q}(\rho) + 3g_{q'q}(\rho)) \quad (26)$$

and averaging out the charge state dependence in a second step,

$$\overline{M}(\rho) = \sqrt{\frac{1}{2}(|M_{pp}(\rho)|^2 + |M_{pn}(\rho)|^2)} . \quad (27)$$

Results for $\overline{M}_{pp}(\rho)$, $\overline{M}_{pn}(\rho)$ and $\overline{M}(\rho)$ are shown in Fig.3. While the short range interaction among equal particles varies only slowly with density, the proton-neutron interaction shows a strong density gradient, reminiscent to the known relations. At saturation density of symmetric nuclear matter, $\rho = \rho_0 = 0.16 \text{ fm}^{-3}$ we find $|\overline{M}(\rho_0)| = 341 \text{ MeV fm}^3$. This value compares extremely well to the independently derived matrix element $|\widetilde{M}| = 320 \text{ MeV fm}^3$ determined in our previous investigations [4, 2, 3] by adjusting the transport theoretical spectral functions to those from the many-body calculations of Benhar et al. [11]. This very gratifying agreement confirms the validity of our approach also for asymmetric matter. Moreover, with the derivation of the relevant interaction matrix element in a theoretically well justified approach we have gained predictive power in regions of total density ρ and for asymmetries $\xi = \rho_p/\rho = Z/A \leq \frac{1}{2}$ which were inaccessible before.

3 Correlations in Asymmetric Nuclear Matter

Spectral functions and the imaginary part of the self-energies have been calculated for nucleons in neutron-rich infinite nuclear matter in the transport

theoretical approach outlined in the previous sections. Results will be displayed at the saturation density $\rho_0 = 0.16 \text{ fm}^{-3}$ of infinite symmetric nuclear matter although with decreasing values of the asymmetry ξ the equilibrium point moves to smaller densities and finally disappears below a critical value of ξ . Our choice of the Lyon-4 parameter set [16] for the Skyrme energy density functional leads to an higher effective mass for protons than for neutrons in neutron-rich matter, i.e. $m_p^*(\rho, \xi) > m_n^*(\rho, \xi)$ for $\xi < \frac{1}{2}$.

The averaged scattering amplitude was chosen according to eq.27, thus accounting for the variation of the average matrix element with density. In all calculations, the real part of the self-energy, which plays an important role for analyticity [2], was included by means of using eq.(4). By numerical reasons the spectral functions were calculated on energy and momentum grids (ω, k) with $-0.5 \text{ GeV} \leq \omega \leq +0.5 \text{ GeV}$ and $0 \leq k \leq 1.5 \text{ GeV}/c$ which obviously leads to a lack of information on the behavior of the spectral functions at energies outside the region covered by the numerical grid. For being able to calculate the $\text{Re}\Sigma_q$ by eq.(4), the imaginary parts were extrapolated into the regions of large energies by assuming Gaussian tails.

The spectral properties of nucleons in asymmetric matter are best explored by keeping the total number density fixed to $\rho = \rho_{eq}$. Then, the average matrix element is $(\overline{|M_{qq'}|^2})^{\frac{1}{2}} = 350 \text{ MeV fm}^3$, being in agreement both with the derivation sketched above and reproducing the spectral functions of ref. [11].

In the imaginary part of the self-energies dynamical correlations are reflected most clearly and directly. Results for $\text{Im}\Sigma_q \equiv \frac{1}{2}\Gamma_q$ are displayed in fig.4 for protons and neutrons ($q=p,n$), respectively, at an asymmetry $\xi = \frac{1}{4}$. The overall dependence of $\text{Im}\Sigma_q$ on energy is constrained by the requirement that the ground state is stationary. Theoretically, this is taken care off by using retarded Green functions, leading to $\text{Im}\Sigma_q(\omega_F(q)) \equiv 0$ as seen in fig.5 and guaranteeing that the ground state is indeed stable as indicated by the vanishing width.

In Fig.5 also results from a recent Brueckner Hartree-Fock (BHF) study of the Tübingen group [6] are included. Both approaches agree qualitatively in the global energy dependence given by a strong increase of $\text{Im}\Sigma_q$ at energies away from the Fermi surface. But in detail, differences are seen to emerge on the quantitative level and especially in the hole sector: While our approach predicts long tails of $\text{Im}\Sigma_q$ extending to large values of $|\omega - \omega_F|$ and eventually levelling off by slowly approaching asymptotic values, the BHF calculations show a much more pronounced fall off at energies deep in the Fermi sea. Such a cutoff behavior is somewhat unexpected at first sight because the density of intermediate ($2h1p$) states still increases with increasing energy

which should overcompensate the suppression introduced by the momentum structure of the interactions. The deviations in the particle sector ($\omega > \omega_F$) are reflecting the differences in the interactions. The BHF calculations are based on the CD-Bonn NN-potential which seems to provide a larger amount of hard scattering at large off-shell momenta than our simplified description using a constant matrix element, obviously not distinguishing between on- and off-shell processes. However, the results of ref.[6] show that similar differences are observed in the BHF calculations when using different NN-potentials. This points to an interesting - and rare - sensitivity of the dynamical self-energies on the off-shell momentum structure of interactions.

In Fig. 6 proton and neutron spectral functions at $\rho = \rho_{eq}$ are displayed for two different momenta and asymmetries $\xi = \frac{1}{2}, \frac{1}{4}$. In all cases, the quasi-particle peaks are clearly identified, as one would expect from symmetric nuclear matter. The main difference to symmetric nuclear matter are in fact the changes in the mean-field due to the isovector self-energy which translate into corresponding changes in the chemical potentials. With increasing neutron excess the protons are bound increasingly stronger while the effective neutron potential becomes shallower, leading to less binding. Hence, the number asymmetry induces via the isovector interactions a gap between the proton and neutron Fermi-surfaces. Hence, both the shape and the location of the peak are influenced by the isovector interactions and their influence on the chemical potentials. This effect, however, is not directly visible in the figure because energies are given with respect to the corresponding Fermi energy. In fact, the results shown in Fig.6 emphasize that the spectral functions depend in the first place on $\omega - \omega_F$.

Comparing the results for $\xi = \frac{1}{4}$ with those for symmetric matter, $\xi = \frac{1}{2}$, we find from fig.6 that in asymmetric matter the proton hole strength functions are moved towards the Fermi level while the proton particle strength is moved away from the Fermi level. The neutron spectral distributions show the complementary behavior: the hole strength is shifted down into the Fermi sea while the particle strength is approaching the Fermi level. This asymmetric behavior is a consequence mainly of the gap between proton and neutron Fermi energies caused by the isovector self-energies. This isovector gap suppresses effectively the coupling of protons to the more abundant neutron ph excitations. Hence, a larger part of the spectral strength is concentrated in the quasi-particle peak. Obviously, within the neutron and proton sectors this effect does not play a role. Therefore, we find larger correlations for neutrons seen as a shift of strength down into the Fermi sea. Interestingly, a considerable part of the different spectral behavior of protons and neutrons is related to their effective masses. This leads to the interesting conclusion that the momentum dependence of the underlying interactions and self-energies

has a significant influence on the spectral properties of asymmetric matter.

Another observation from Fig.6 is that the width of the quasi-particle peaks decreases when approaching the Fermi surface. This is in agreement with the general expectation that closer to the Fermi surface the life time of quasi-particle states increases strongly. The energy-momentum structure of $\Gamma(\omega, k)$ is illustrated in fig.4 for two momentum cuts in symmetric and asymmetric matter. From the behavior of $\Gamma(\omega, k)$ we conclude that in asymmetric matter the collision rates in the hole sector increase for neutrons while for protons they slightly decreases. For either type of nucleon the amount of correlations decrease for states above the Fermi level compared to symmetric matter. The reason behind this behavior is again found in the differences in level densities and Fermi energies.

In Fig.7 and Fig.8 spectral functions for an asymmetry $\xi = \frac{1}{4}$ and at total densities between half and twice nuclear saturation density $\rho_{eq} = 0.16 \text{ fm}^{-3}$ are displayed. In Fig.7 the spectral distribution of a nucleon well inside the Fermi sea is shown. The evolution of the spectral functions with density are partly related to the change in chemical potential. At $\rho = \frac{1}{2}\rho_{eq}$ a state with the chosen momentum is much closer to the Fermi surface than for $\rho = \rho_{eq}$ or $\rho = 2\rho_{eq}$. This explains the variation in width and position of the quasi-particle peak seen in Fig.7.

In Fig.8 spectral functions for a particle state well above the Fermi surface are shown. Again, with increasing density the relative distance of the quasi-particle from the Fermi surface decreases and this dependence is reflected in the shift and the reduction of the width at higher density. In both cases, long spectral tails in the region below or above the Fermi surface, respectively, are found, indicating a considerable shift of single particle strength away from the quasi-particle peak. The overall features, however, are qualitatively similar to those observed previously in symmetric nuclear matter [2, 3] although the results differ on the quantitative level.

We finally consider the proton and neutron ground state momentum distributions

$$n_q(k) = \int_{-\infty}^{\mu_q} d\omega a(\omega, k) \quad (28)$$

where μ_q is the chemical potential for nucleons of type $q = p, n$. Results for symmetric and asymmetric nuclear matter are shown in Fig.9. There, the shrinking of the proton Fermi sphere in neutron-rich matter is clearly visible in the diminished region of occupied proton momentum states. In asymmetric matter the structure of the momentum distributions follows otherwise closely the same pattern as found already in symmetric matter: Inside the Fermi sea the occupancy is reduced by about 10% and this fraction of the spectral strength is shifted into a high momentum tail with an almost exponential

decline. At first sight it seem surprising to find that at high momenta the distributions approach the each other showing very similar magnitudes and slopes. However, this result is another illustration of the universality of the dynamical short range correlations which already was found in our previous investigations [4, 2, 3].

4 Summary and Outlook

Dynamical correlations in asymmetric infinite nuclear matter were investigated in a transport theoretical approach, thereby extending our previous work into a new regime. It is worthwhile to emphasize that only few studies on dynamical correlations in asymmetric exist. In asymmetric matter isovector effects are strongly enhanced with increasing asymmetry. On the mean-field level this was taken into account by using a modern Skyrme energy density functional from the Lyon group [16] with parameters adjusted both to finite nuclei and neutron stars. In this sense, we describe the evolution of mean-field dynamics with asymmetry and density in a realistic model. In particular, the saturation properties of infinite nuclear matter are well described. Using Landau-Migdal theory we could derive from the Skyrme functional the corresponding effective quasi-particle interaction in a self-consistent way. An approach was presented which allows to extract the short-range interactions by subtracting the pion exchange contributions.

The overall features of Self-energies and spectral functions in asymmetric nuclear matter resemble those found in our previous work on short range correlations in symmetric matter. In particular, the present investigation confirms our previous conclusion on the universal character of short range correlations in infinite nuclear matter. An interesting observation in the present context is the sensitivity of the spectral distributions on the momentum structure of self-energies and interactions.

Acknowledgments

We thank F. Frömel for helpful discussions and numerical hints during preparation of this work.

A Landau-Migdal parameters for the pion

Second variation of the energy density in equation (16) with respect to spin and isospin densities leads to

$$\begin{aligned} \frac{\partial^2 E_\pi(\rho)}{\partial \rho_q \partial \rho_{q'}} &= \sum_{S,T=0,1} [V_{ST}(k_f(q), k_f(q')) (\vec{\sigma}_1 \cdot \vec{\sigma}_2)^S (\vec{\tau}_1 \cdot \vec{\tau}_2)^T \\ &+ \frac{1}{k_f(q')^2} \sum_{q''} \int dk k^2 \Theta(k_f(q'') - k) \frac{\partial}{\partial q} |_{k_f(q')} V_{ST} < (\vec{\sigma}_1 \cdot \vec{\sigma}_2)^S (\vec{\tau}_1 \cdot \vec{\tau}_2)^T >] \end{aligned} \quad (29)$$

where the brackets indicate ground state expectation values. From which we now identify the Landau-Migdal parameters:

$$f^{(\pi)} = N_0(k_f) V_{00} + f^r(k_f) \quad (30)$$

$$f'^{(\pi)} = N_0(k_f) V_{10} \quad (31)$$

$$g^{(\pi)} = N_0(k_f) V_{01} \quad (32)$$

$$g'^{(\pi)} = N_0(k_f) V_{11} \quad (33)$$

where $f^r(k_f)$ is an rearrangement term, which appears for spin-saturated symmetric nuclear matter only in the $S = 0, T = 0$ channel. Expansion of the in-medium scattering amplitude in a Legendre series, which is common, leads to

$$f_l^{(\pi)} = \frac{1}{2} \int_{-1}^1 P_l(\cos \theta) f^\pi(\cos \theta) d\cos \theta. \quad (34)$$

The integration over the angle θ is done using the Newman formula

$$Q_l(t) = \frac{1}{2} \int_{-1}^1 \frac{P_l(x)}{t - x} dx \quad (35)$$

where the $Q_l(t)$ are Legendre polynomials of the 2nd kind. Using equation (35) together with our expressions for the Landau-Migdal parameters leads to

$$f_l^{(\pi)} = -4\pi \frac{9}{4} N_0(k_F) \frac{f_\pi^2}{2k_F^2} Q_l(1 + \frac{m_\pi^2}{2k_F^2}) + f_l^{(r)}(k_F) \quad (36)$$

$$f_l'^{(\pi)} = 4\pi \frac{3}{4} N_0(k_F) \frac{f_\pi^2}{2k_F^2} Q_l(1 + \frac{m_\pi^2}{2k_F^2}) \quad (37)$$

$$g_l^{(\pi)} = 4\pi \frac{3}{4} N_0(k_F) \frac{f_\pi^2}{2k_F^2} Q_l(1 + \frac{m_\pi^2}{2k_F^2}) \quad (38)$$

$$g_l'^{(\pi)} = g'_H \delta_{l0} - 4\pi \frac{1}{4} N_0(k_F) \frac{f_\pi^2}{2k_F^2} Q_l(1 + \frac{m_\pi^2}{2k_F^2}). \quad (39)$$

where the $l = 0$ components in the $S = 1, T = 1$ channel includes in addition the direct (i.e. Hartree-type) contributions

$$g'_H = 4\pi N_0(k_F) \frac{f_\pi^2}{m_\pi^2} \quad (40)$$

For the additional rearrangement term in equation (36) we get

$$f^{(r)}(k_F) = N_0(k_F) \frac{1}{k_F^2} \int dk k^2 \Theta(k_F - k) \frac{\partial}{\partial q} V_0^{(\pi)}(k, k') \quad (41)$$

where $V_0^\pi(k, k')$ is the monopol component of the $S = 0, T = 0$ u-channel pion exchange interaction.

References

- [1] W. Dickhoff, C. Barbieri, *Prog.Part.Nucl.Phys.* **52** (2004) 377-496.
- [2] J. Lehr, M. Effenberger, H. Lenske, S. Leupold, U. Mosel, *Phys. Lett.* **B483** (2000) 324.
- [3] J. Lehr, H. Lenske, S. Leupold, U. Mosel, *Nucl. Phys.* **A703** (2002) 393.
- [4] F. Froemel, H. Lenske, U. Mosel, *Nucl. Phys.* **A723** (2003) 544.
- [5] P. Bozek, *Phys.Lett.* **B586** (2004) 239-243.
- [6] Kh.S.A. Hassaneen, H. Müther, [arXiv:nucl-th/0408035](https://arxiv.org/abs/nucl-th/0408035).
- [7] D. Cortina-Gil, T. Baumann, H. Geissel, K. Sümmerer, L. Axelson, U. Bergmann, M.J.G. Borge, L. Fraile, M. Hellström, M. Ivanov, N. Iwasa, R. Janik, B. Jonson, H. Lenske, K. Markenroth, G. Münzenberg, F. Nickel, T. Nilsson, A. Ozawa, K. Riisager, G. Schrieder, W. Schwab, H. Simon, C. Scheidenberger, B. Sitar, M. Smedberg, P. Strmen, T. Suzuki, M. Winkler, *Eur.Phys.J A10* 49 (2001).
- [8] D. Cortina-Gil, K. Markenroth, F. Attallah, T. Baumann, J. Benlliure, M.J.G. Borge, L.V. Chulkov, U. Datta Pramanik, J. Fernandez-Vazquez, C. Forssn, L.M. Fraile, H. Geissel, J. Gerl, F. Hammache, K. Itahashi, R. Janik, B. Jonson, S. Karlsson, H. Lenske, S. Mandal, M. Meister, X. Mocko, G. Mnzenberg, T. Ohtsubo, A. Ozawa, Y. Parfenova, V. Pribora, K. Riisager, H. Scheit, R. Schneider, K. Schmidt, G. Schrieder, H. Simon, B. Sitar, A. Stoltz, P. Strmen, K. Sümmerer, I. Szarka, S. Wan, H. Weick and M. Zhukov, *Phys.Lett.* **B529** (1-2) (2002) pp. 36-41.
- [9] H. Lenske, F. Hofmann, C.M. Keil, *Rep.Prog.Nucl.Part.Phys.* **46** (2001) 187, e-Print Archive: [nucl-th/0012082](https://arxiv.org/abs/nucl-th/0012082).
- [10] H. Lenske, C.M. Keil, Nadia Tsoneva, *Prog.Part.Nucl.Phys.* **53** (2004) 153.
- [11] O. Benhar, A. Fabrocini, S. Fantoni, *Nucl. Phys.* **A505** (1989) 267; O. Benhar, A. Fabrocini, S. Fantoni, *Nucl. Phys.* **A550** (1992) 741.
- [12] L.P. Kadanoff and G. Baym, *Quantum Statistical Mechanics* (Benjamin, New York, 1962).
- [13] A. B. Migdal, *Theory of Finite Fermi Systems and Applications to Atomic Nuclei* (Interscience, New York, 1975).

- [14] M. Bender, J. Dobaczewski, J. Engel, W. Nazarewicz, Phys. Rev. **C85** (2002) 054322.
- [15] I. Bombaci, U. Lombardo Phys. Rev. **C44** (1991) 1892.
- [16] E. Chabanat, P. Bonche, P. Haensel, J. Meyer, R. Schaeffer, Nucl. Phys. **A627** (1997) 710.

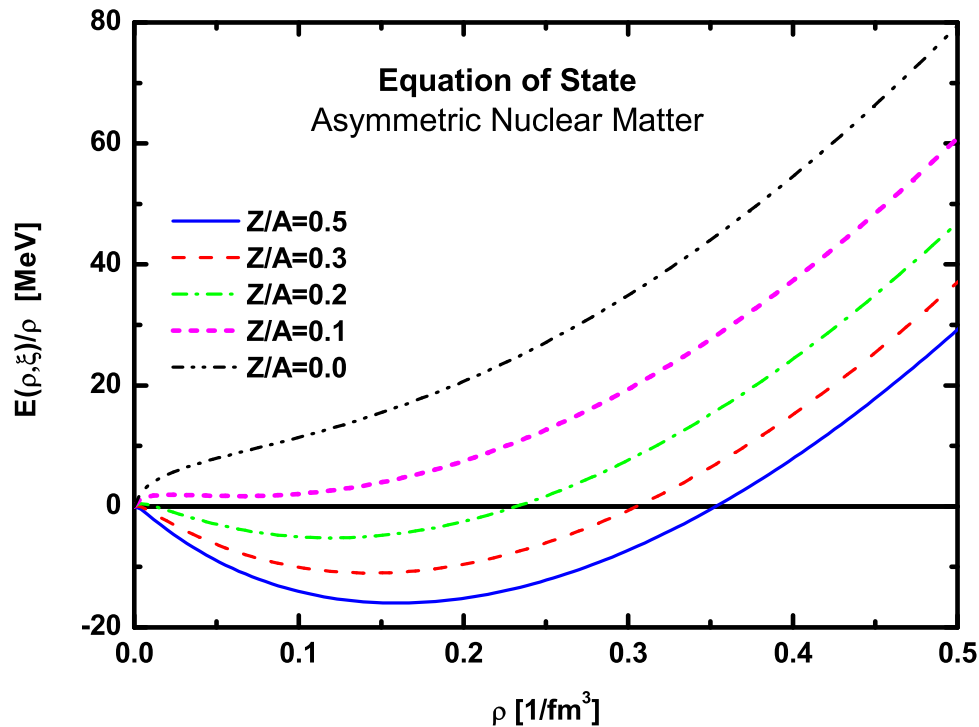


Figure 1: Equation of state of infinite nuclear matter at various asymmetries $\xi = \rho_p/\rho = Z/A$. Results obtained with the Lyon-4 parameter set [16] are shown.

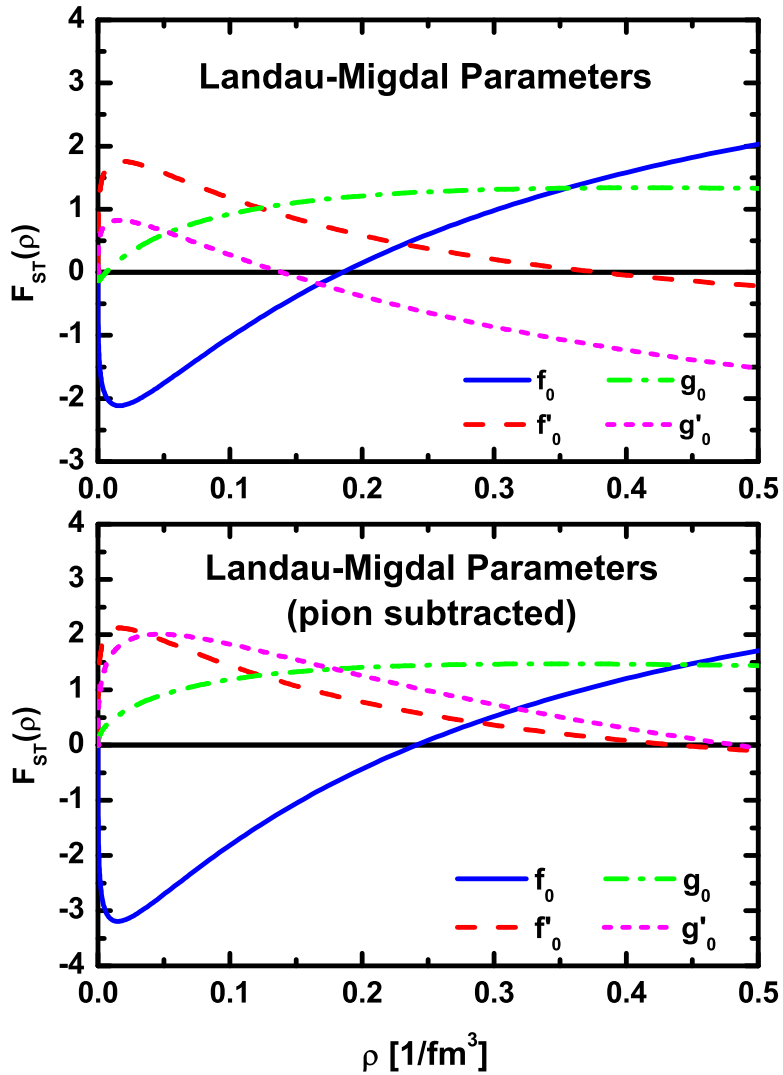


Figure 2: Landau-Migdal parameters in symmetric nuclear matter for the full Lyon-4 interaction (upper panel) [16] and the pion-subtracted short range interaction (lower panel).

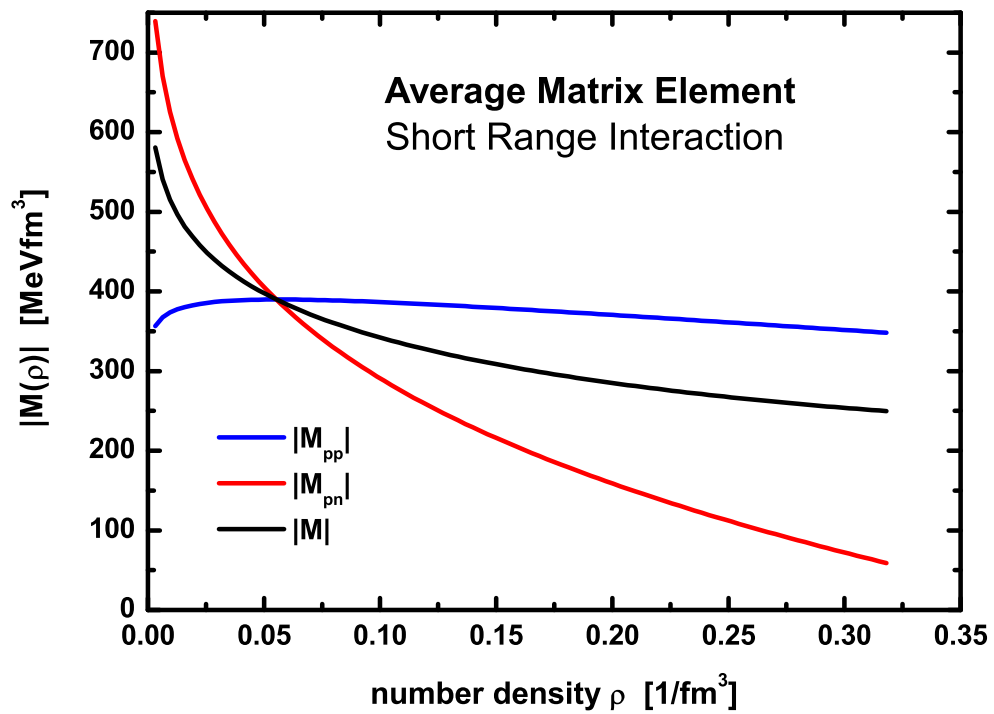


Figure 3: Dependence of the average short range interaction matrix elements $|M_{qq'}$ and of the average matrix element \overline{M} , eq.27, on density in infinite nuclear matter.

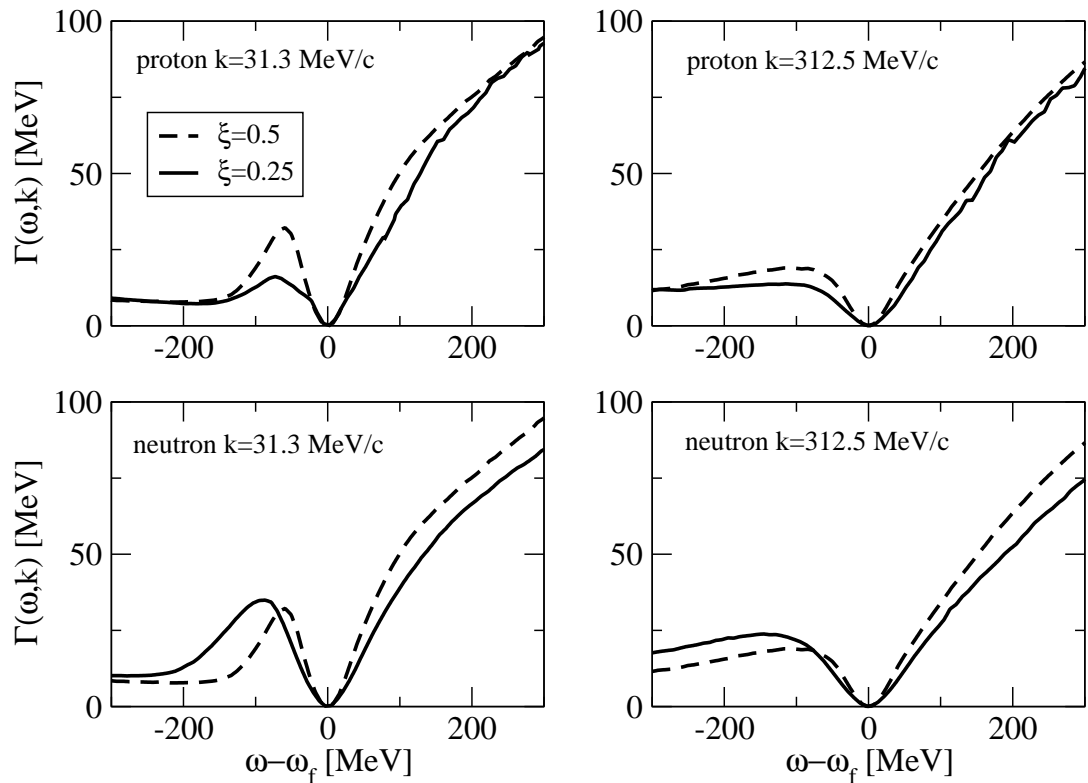


Figure 4: The nucleon width for symmetric (dashed line) and asymmetric nuclear matter (straight line). The upper graphs refer to protons the lower ones to neutrons.

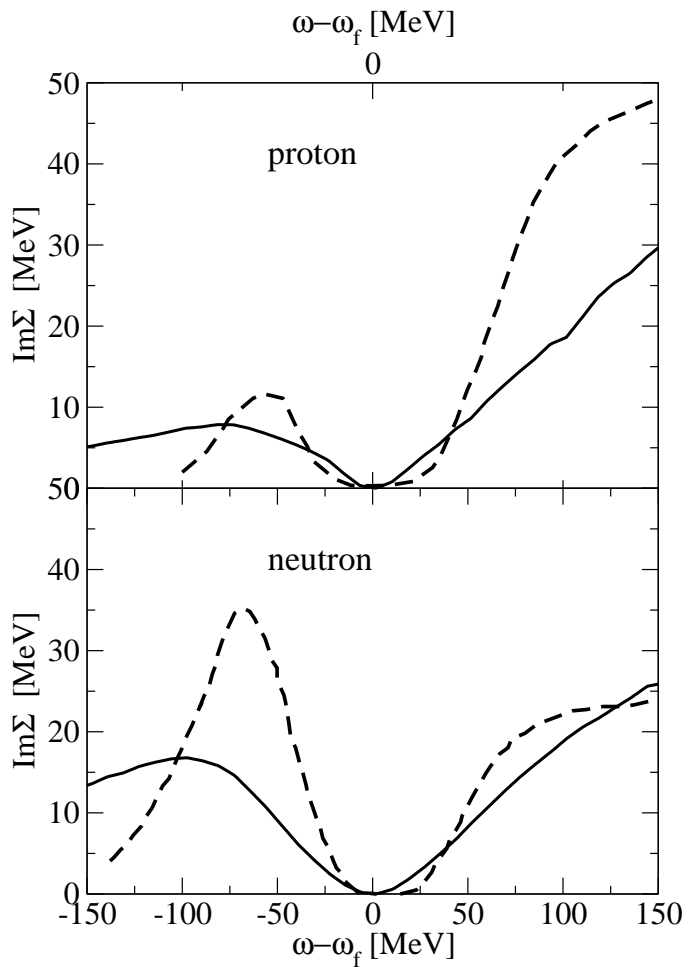


Figure 5: The imaginary part of the nucleon self-energy for momentum $k = 0.4k_f$ and asymmetry $\xi = 0.25$ at a density $\rho = 0.17$ $1/fm$. The dotted line represents the results from [6].

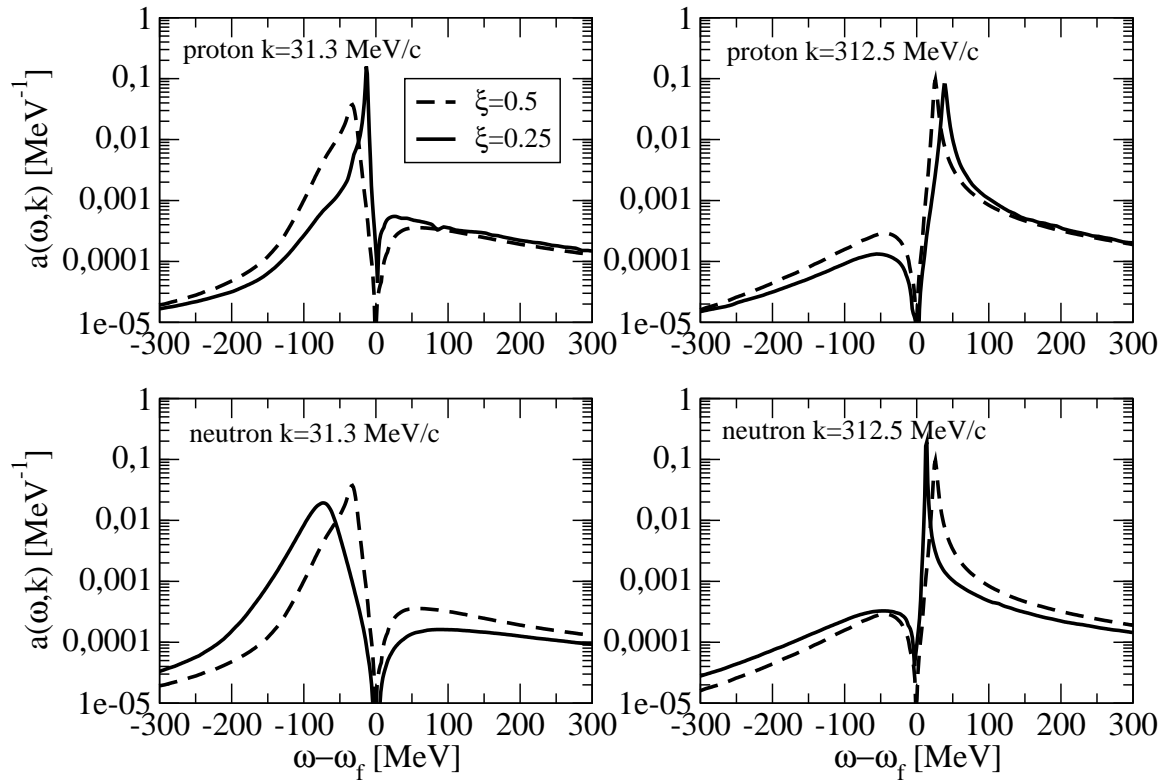


Figure 6: The nucleon spectral function for symmetric and asymmetric nuclear matter. The dashedline refers to symmetric and the straight line to asymmetric nuclear matter with an asymmetry of $\xi = 0.25$. The upper graphs show the results for protons, the lower ones the results for neutrons.

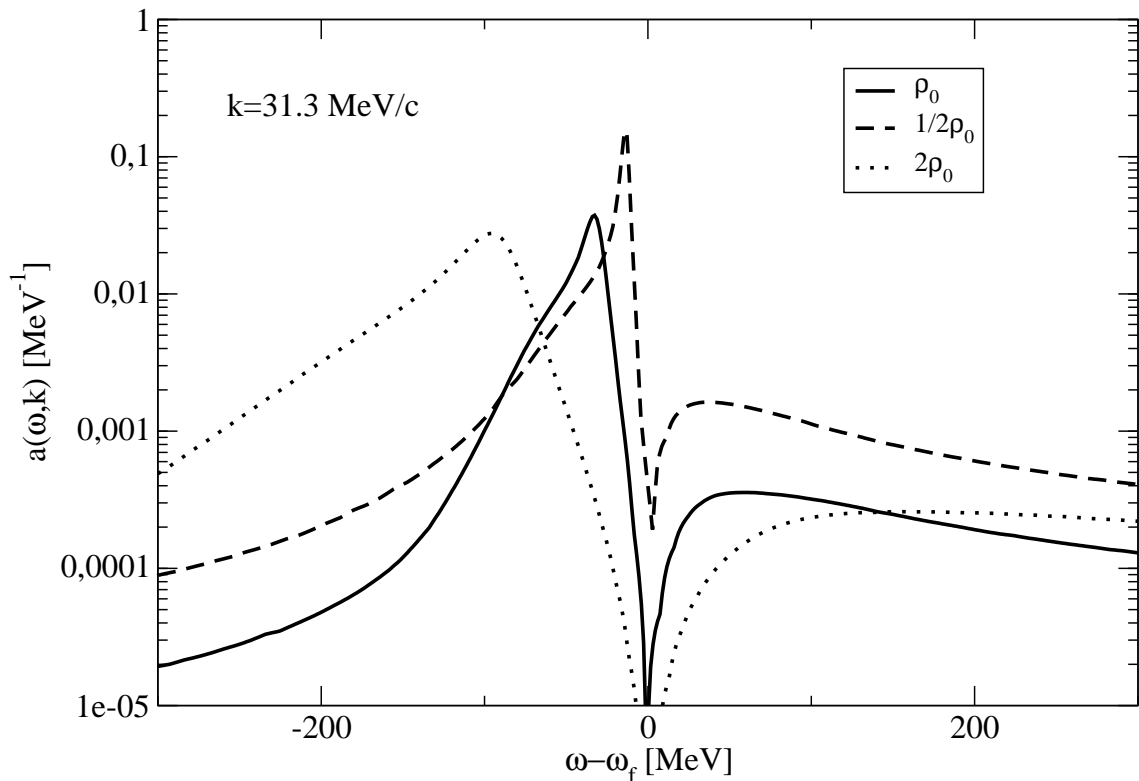


Figure 7: Spectral functions of a nucleon well inside the Fermi sea at density $\rho = \frac{1}{2}\rho_{eq}$, $\rho = \rho_{eq}$ and $\rho = 2\rho_{eq}$.

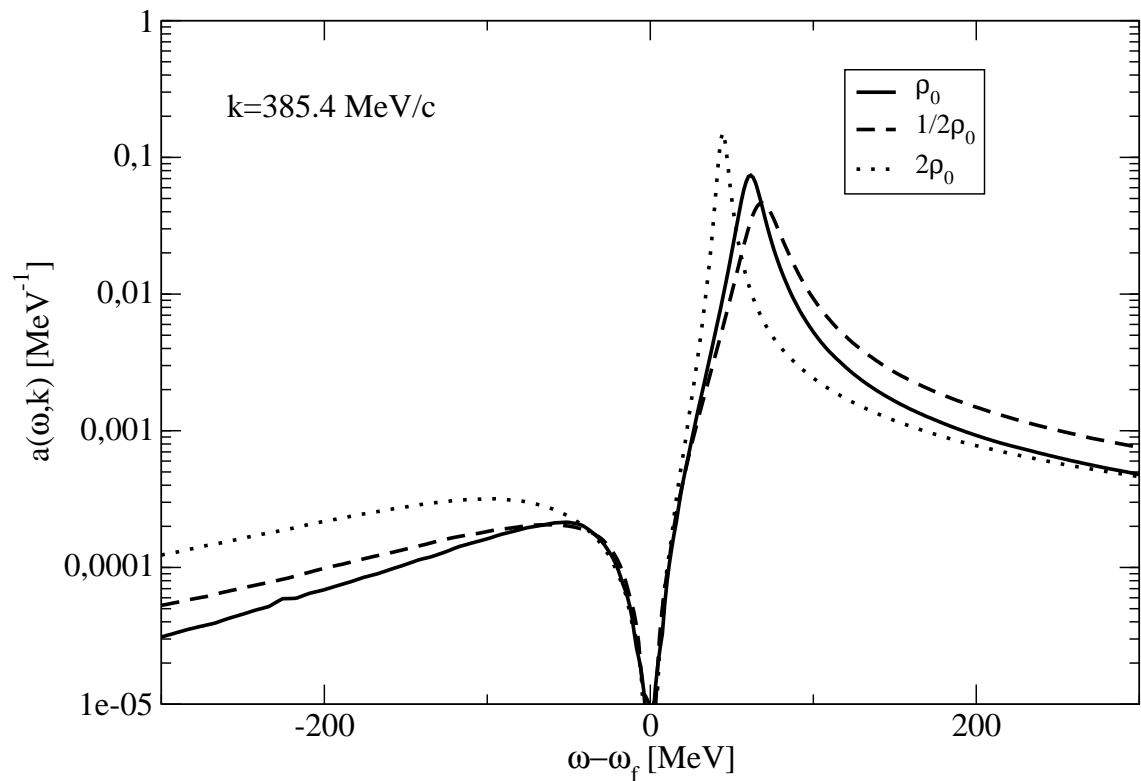


Figure 8: Spectral functions of a nucleon well outside the Fermi sea at density $\rho = \frac{1}{2}\rho_{eq}$, $\rho = \rho_{eq}$ and $\rho = 2\rho_{eq}$.

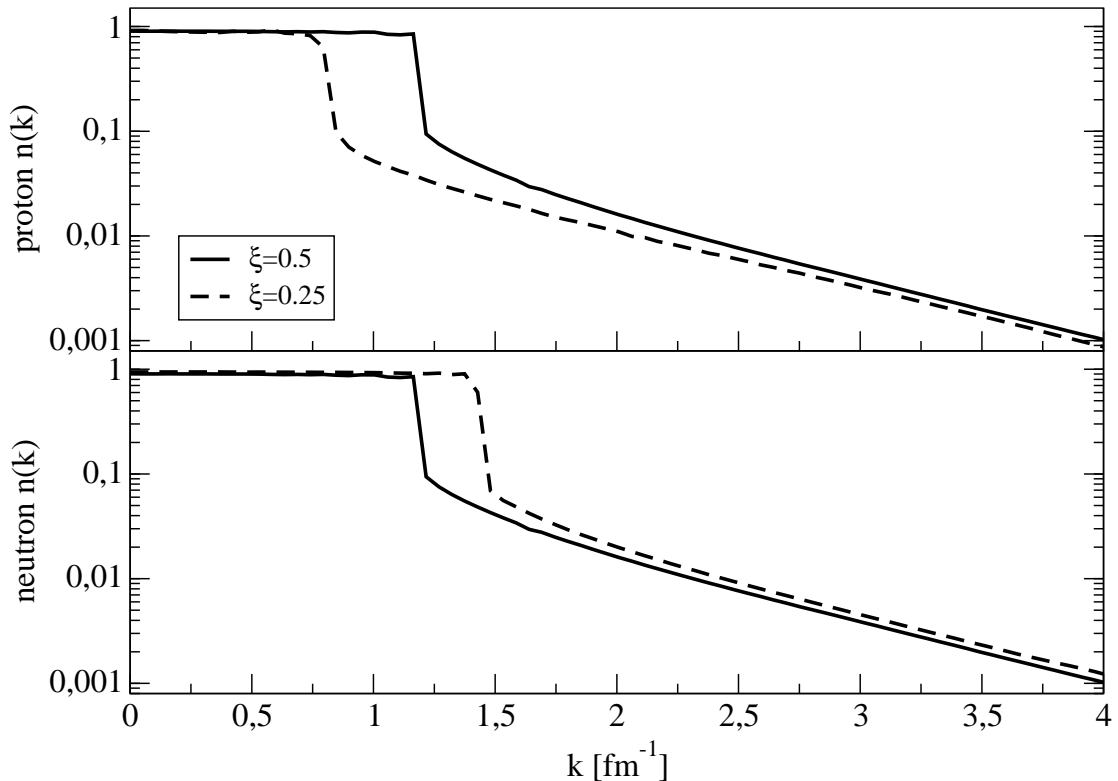


Figure 9: The momentum distribution for protons (upper graph) and neutrons (lower graph). The straight line is the result for symmetric nuclear matter the dashed line for asymmetric nuclear matter ($\xi = 0.25$)